energies

MDPI

Article

Thermodynamic Insight in Design of Methanation Reactor with Water Removal Considering Nexus between CO_2 Conversion and Irreversibilities

Sayed Ebrahim Hashemi [1,*], Kristian M. Lien [1], Magne Hillestad [2], Sondre K. Schnell [3] and Bjørn Austbø [1]

[1] Department of Energy and Process Technology, Norwegian University of Science and Technology (NTNU), NO-7491 Trondheim, Norway; kristian.m.lien@ntnu.no (K.M.L.); bjorn.austbo@ntnu.no (B.A.)
[2] Department of Chemical Engineering, Norwegian University of Science and Technology (NTNU), NO-7491 Trondheim, Norway; magne.hillestad@ntnu.no
[3] Department of Material Science and Engineering, Norwegian University of Science and Technology (NTNU), NO-7491 Trondheim, Norway; sondre.k.schnell@ntnu.no
* Correspondence: ebrahim.hashemi@ntnu.no

Abstract: The inevitable nexus between energy use and CO_2 emission necessitates the development of sustainable energy systems. The conversion of CO_2 to CH_4 using green H_2 in power-to-gas applications in such energy systems has attracted much interest. In this context, the present study provides a thermodynamic insight into the effect of water removal on CO_2 conversion and irreversibility within a CO_2 methanation reactor. A fixed-bed reactor with one intermediate water removal point, representing two reactors in series, was modeled by a one-dimensional pseudo-homogeneous model. Pure CO_2 or a mixture of CO_2 and methane, representing a typical biogas mixture, were used as feed. For short reactors, both the maximum conversion and the largest irreversibilities were observed when the water removal point was located in the middle of the reactor. However, as the length of the reactor increased, the water removal point with the highest conversion was shifted towards the end of the reactor, accompanied by a smaller thermodynamic penalty. The largest irreversibilities in long reactors were obtained when water removal took place closer to the inlet of the reactor. The study discusses the potential benefit of partial water removal and reactant feeding for energy-efficient reactor design.

Keywords: methanation; water removal; reactor design; CO_2 conversion; irreversibility

Citation: Hashemi, S.E.; Lien, K.M.; Hillestad, M.; Schnell, S.K.; Austbø, B. Thermodynamic Insight in Design of Methanation Reactor with Water Removal Considering Nexus between CO_2 Conversion and Irreversibilities. *Energies* **2021**, *14*, 7861. https://doi.org/10.3390/en14237861

Academic Editor: Pouya Ifaei

Received: 31 October 2021
Accepted: 18 November 2021
Published: 24 November 2021

1. Introduction

Economic growth, energy use, and CO_2 emissions are associated with one another. He et al. [1] stated that rapid growth in the economy and energy use has caused an increase in CO_2 emissions. Pao and Tsai [2] investigated the economy-energy-sustainability nexus. They illustrated that the reduction of CO_2 emission without negative effect on the economic growth could obtain by increasing energy efficiency. Balsalobre et al. [3] pointed out that the implementation of energy strategies that emphasizes shifting towards renewable energy sources could effectively reduce the dependency on fossil fuels, and thereby also reduce CO_2 emissions.

In modern energy systems, an increased share of renewable energy sources like solar and wind has been seen as a solution for mitigating CO_2 emissions [4]. However, the intermittent nature of renewable energy sources entails a need to consider energy storage when renewable power generation does not match the demand [5]. Among possible energy storage technologies [5,6], Power-to-Gas (PtG) concepts provide the possibility of converting surplus renewable electricity to chemical energy through the production of energy carrier components such as hydrogen (H_2), methane (CH_4), and methanol (CH_3OH) [7].

Essentially, the production of H_2 from water electrolysis run by surplus renewable electricity is considered the first step in these PtG applications. The production of H_2 from renewable energy has multiple advantages such as low harmful emissions fewer steps of energy conversion to produce alternative fuel from renewable electricity, and direct utilization in fuel cell vehicles. Nonetheless, lacking storage capacity and distribution infrastructure limit the use of H_2 [8]. An alternative is the further chemical conversion of the H_2 into other energy carriers, e.g., CH_4 or CH_3OH. Although the overall process efficiency is reduced by additional chemical conversion steps, higher energy density and mature infrastructure motivate the use of alternatives [9]. Moreover, CH_4 is used for power generation, transportation, and as a precursor for other chemicals [9,10]. In PtG applications, the methane is produced through catalytic or biological methanation using CO_2 from renewable carbon sources such as biogas, or captured CO_2 from industrial processes, and H_2 from water electrolysis.

In catalytic methanation, CO_2 reacts with H_2, in the presence of a catalyst, through a reversible and highly exothermic reaction, known as the Sabatier reaction, producing CH_4 and water (H_2O) [11].

$$CO_2 + 4H_2 \rightleftharpoons CH_4 + 2H_2O \qquad (\Delta H^{\circ}_{298\ K} = -165\ kJ/mol) \tag{1}$$

Although methanation has been in use for many years in different industries like ammonia production plants and synthetic natural gas (SNG) production, the development of the methanation reactor design is still an attractive topic in research to improve the performance of the methanation process in terms of CO_2 conversion, cost efficiency, and stability of the reactor with respect to the load fluctuation from renewable sources [12]. The traditional methanation reactors are fixed-bed reactors (FBR) [13–18] and fluidized bed reactors [19–21]. Recently, three-phase slurry reactors [22–24] and microchannel reactors [25,26] have also been developed for the methanation process. Inclusive reviews of the mentioned reactor concepts can be found in the literature [7,12]. The majority of commercial CO_2 methanation processes are based on catalytic FBR, operating under adiabatic conditions in a series of reactors with intermediate cooling or operating under isothermal conditions [12]. Hashemi et al. [27] indicated that the operation of the methanation process in a series of adiabatic reactors would reduce the irreversibility rate within the reactors, in comparison with isothermal reactors, improving the process integration potentials.

One important aspect of the methanation reactor design is the highly exothermic nature of the CO_2 methanation reaction, and many reactor concepts have been developed to overcome challenges regarding heat management and temperature control along the reactor [12]. Optimal heat management within the reactor can lead to higher CO_2 conversion. Sun et al. [28] performed a simulation-based study considering a kinetic model for the CO_2 methanation in an FBR to observe the effect of heat removal on the methane yield. They proposed a new design configuration with a molten salt-cooled heat exchanger to improve the cooling rate within the reactor, leading to increased methane yield. In another work by Sun et al. [29], it was observed that the molten salt flow rate, which indicated the cooling rate, was a crucial parameter for the reactor performance. They observed that the methane yield improved with reduced temperature (increased cooling rate), but also that overcooling would hinder the reaction. Moreover, they demonstrated that although the methane yield improved by increasing the space velocity, there was a threshold above which further increase in the space velocity led to reduced conversion. Kiewidt and Thöming [30] proposed a method to optimize the temperature profile within an FBR by balancing the heat production rate and the cooling rate. They illustrated that the methane yield improved by optimizing the temperature profile. Their results demonstrated that the optimal temperature profile was located between the temperature profiles obtained from isothermal and adiabatic operations, when balancing the kinetics and thermodynamic limitations along the reactor.

In PtG applications, it is essential to convert as much H_2 as possible since it is a major driving factor for the cost [29]. Improving the hydrogen conversion is equivalent

to improving the CO_2 conversion for a given amount of hydrogen. Besides the reactor design aspects concerning heat management within the reactor, many studies regarding reactor design focus on CO_2 conversion improvement by manipulating thermodynamic equilibrium within the reactor.

Water removal in the methanation process can shift the thermodynamic equilibrium of the Sabatier reaction towards the product side, enhancing the CO_2 conversion. Recently, this has triggered reactor concepts such as sorption enhanced methanation (SEM) and water-selective membrane reactors (MR) [9,31]. Within SEM and MR concepts, the produced H_2O in the methanation process is locally removed from the gas phase stream within the reactor by means of sorption materials such as zeolite and silica. A complete overview regarding SEM and MR with respect to sorption materials and reactor configuration design can be found in the work by van Kampen et al. [32] and Diban et al. [33], respectively.

Walspurger et al. [34] investigated the effect of water removal in an SEM reactor experimentally. They indicated that a CO_2 conversion near to 100% was possible in an SEM reactor with a commercial nickel-based catalyst and zeolite 4A as H_2O adsorbent when the operating temperature was between 250 and 350 °C. Based on Gibbs' free energy minimization, Faria et al. [35] studied in-situ water removal in an equilibrium model methanation reactor. In addition to the species present in the Sabatier reaction, they also included carbon monoxide and coke in their simulations. They illustrated that the CO_2 conversion increased with increasing water removal fraction, independently of the operating temperature and pressure. However, the methane yield was maximized at an optimal water removal fraction, depending on the temperature and pressure, above which coke formation was observed [35]. Najari et al. [36] investigated the effect of in-situ water removal from a methanation reactor using kinetic models. They illustrated that removing water locally improved the reactor performance in terms of conversion, but this also increased the risk of hot spots within the reactor, which could have a negative impact on the functionality of the catalysts [36]. Their study suggested that further examination of the effects of kinetics and temperature on the reactor performance was required [36].

Although in-situ water removal provides apparent advantages for the methanation process from a thermodynamic point of view, practical aspects, such as heat management and membrane characterization, must also be considered [32]. For reactors operated in series, as previously mentioned, water may be removed in between the stages, as an alternative to in-situ water removal. This suggests investigating the effect of water removal in stages can be considered an alternative to continuous water removal through SEM or MR. Hillestad [37] proposed a systematic staging method for the design of chemical reactors. He demonstrated that staging provided additional degrees of freedom to obtain better performance in the reactor.

Even though water removal between the methanation reactor stages has been considered as a method to increase the CO_2 conversion, investigation regarding how the design of staging with intermediate water removal should consider the reactor length (i.e., representing reactor volume) is missing in the literature. In this regard, the optimal water removal location point is expected to be dependent on the length of the reactor. Further, the energy efficiency of methanation reactors with intermediate water removal has received limited attention in the literature; most research studies in the field of reactor design emphasize performance improvement in terms of CO_2 conversion and heat management. The present study aims to fill these research gaps by conducting a fundamental thermodynamic study to examine the concept of water removal for different reactor lengths. The optimal water removal point within a reactor is determined for different operating conditions. The performance of the reactor is assessed in terms of improvement in the CO_2 conversion. Moreover, alternative objectives related to the total irreversibility within the reactor and the minimum required work for water removal are also discussed.

In Section 2, the reactor model development, reaction kinetics, and numerical solution strategy for the model are given. The methods employed to investigate the effect of water removal at different locations along the reactor are explained in Section 3. Further, a de-

scription regarding the calculation of irreversibility rate and minimum work requirements for water removal is presented. Results for the optimal location for water removal in the reactor with respect to conversion and irreversibility are presented in Section 4. Remarks and suggestions for further studies are provided in Section 5. Finally, conclusions are presented in Section 6.

2. Model Development

According to the conclusions drawn by Fischer et al. [38], a simplified one-dimensional pseudo-homogenous model, known as a plug flow reactor (PFR) model, provides sufficient accuracy to predict the CO_2 conversion within an FBR. In the present study, the pseudo-homogeneous model was combined with an effectiveness factor to accommodate the intra-particle mass and heat transport limitations between solid (catalyst pellets) and fluid (gas mixtures) phases [30]. Here, it was assumed that a concept similar to the isothermal reactor concept developed by Linde can provide isothermal operating conditions for the methanation [39]. However, it should be noted that operating under isothermal conditions is a challenging task in practice, and might not be economically feasible, as the highly active catalyst causes large heat production and potential hot spots in the reactor. The irreversibility associated with heat transfer may contribute significantly to overall process irreversibility. Test simulations within this study showed that the pressure drop along the reactor length (obtained from the Ergun equation) was on a scale of 0.1 kPa for the studied dimension and flow rates. Therefore, the pressure drop in the reactor was neglected in the PFR model, to focus on the variation of driving forces caused by reaction along the reactor. Further, the ideal gas law was applied as an equation of state. The mathematical model for the FBR is presented in the following subsections.

2.1. Reactor Modeling

The FBR in the present study was modeled by considering a plug flow reactor [40] assuming steady-state conditions. In the plug flow assumption, gradients of temperature and concentration are only considered in the axial direction, not the radial direction or the angular direction. Material balances for all the chemical substances involved along the length of the reactor (CO_2, H_2, CH_4, and H_2O) can be expressed as

$$\frac{\mathrm{d}F_i}{\mathrm{d}x} = \rho_c \cdot (1-\varepsilon) \cdot A_c \cdot \eta \cdot \nu_i \cdot r. \tag{2}$$

Here, F_i is the molar flow rate of component i in the direction x along the reactor, while ρ_c, ε, and A_c denote the catalyst density, the void fraction, and the cross-sectional area of the reactor, respectively. Further, ν_i is the stoichiometric coefficient of component i in reaction (1). Explicit expressions for the reaction rate (r) and the effectiveness factor (η) are given in the following subsections.

2.2. Reaction Kinetics

The kinetic model of Koschany et al. [41], where the CO_2 methanation reaction over a Ni-based catalyst is considered, was used in this work. The reaction kinetics, and thereby the CO_2 conversion, is influenced by the operating temperature, pressure, and inlet gas mixture composition. The reaction rate model of Koschany et al. [41] can be applied in temperature and pressure ranges of 180–340 °C and 1–15 bar, respectively. Under these conditions, the CO methanation through reverse-water-gas-shift (RWGS) is limited; hence considering only the CO_2 methanation reaction is reasonable [42]. The reaction rate is based on a Langmuir-Hinshelwood-Hougen-Watson approach as follows:

$$r = \frac{k \cdot p_{H_2}^{0.5} \cdot p_{CO_2}^{0.5} \cdot \left(1 - \frac{p_{CH_4} \cdot p_{H_2O}^2}{p_{CO_2} \cdot p_{H_2}^4 \cdot K_{eq}}\right)}{\left(1 + K_{OH} \cdot \frac{p_{H_2O}}{p_{H_2}^{0.5}} + K_{H_2} \cdot p_{H_2}^{0.5} + K_{mix} \cdot p_{CO_2}^{0.5}\right)^2}. \tag{3}$$

Here, p_i is the partial pressure of component i. The rate constant (k) and adsorption constants (K_j) are calculated in accordance with Arrhenius and van 't Hoff-type equations, respectively, as follows:

$$k = k_{ref} \cdot \exp\left(\frac{E_a}{R} \cdot \left(\frac{1}{T_{ref}} - \frac{1}{T}\right)\right), \quad (4)$$

$$K_j = K_{j,ref} \cdot \exp\left(\frac{\Delta H_j}{R} \cdot \left(\frac{1}{T_{ref}} - \frac{1}{T}\right)\right). \quad (5)$$

Here, E_a and ΔH are activation energy and enthalpy of adsorption, respectively. T and R are the temperature and the universal gas constant, respectively. The equilibrium constant (K_{eq}) is approximated as [43]

$$K_{eq} = 137 \cdot T^{-3.998} \cdot \exp\left(\frac{158.7 \frac{kJ}{mol}}{RT}\right). \quad (6)$$

The values of the kinetic model parameters are given in Table 1.

Table 1. Values of kinetics model parameters [41].

Variable	T_{ref}	k_{ref}	E_a	$K_{OH,ref}$	ΔH_{OH}	$K_{H_2,ref}$	ΔH_{H_2}	$K_{mix,ref}$	ΔH_{mix}
Unit	K	mol/bar·s·kg_{cat}	kJ/mol	$bar^{-0.5}$	kJ/mol	$bar^{-0.5}$	kJ/mol	$bar^{-0.5}$	kJ/mol
Value	555	$3.46 \cdot 10^{-1}$	77.5	0.5	22.4	0.44	−6.2	0.88	−10

2.3. Effectiveness Factor

In comparison to CO_2, H_2 diffuses much faster into the catalyst pellets. Thereby, an adopted Thiele modulus can be used to calculate the effectiveness factor, assuming CO_2 to be the limiting species for intra-particle mass transport [30]. The effectiveness factor for spherical catalyst pellets is given as

$$\eta = \frac{3}{\phi}\left(\frac{1}{\tanh\phi} - \frac{1}{\phi}\right), \quad (7)$$

where the Thiele modulus (ϕ) can be calculated considering CO_2 as the key species in the determination of the mass transfer limitations:

$$\phi = \frac{D_p}{2}\sqrt{\frac{r \cdot \rho_c \cdot (1-\varepsilon) \cdot R \cdot T}{D^{eff}_{CO_2} \cdot y_{CO_2} \cdot p \cdot 10^5}}. \quad (8)$$

Here, D_p and y_{CO_2} denote the catalyst pellets diameter and the mole fraction of CO_2 in the gas mixture, respectively. The effective CO_2 diffusivity ($D^{eff}_{CO_2}$) is calculated according to the Bosanquet equation taking into account molecular diffusion ($D^{m}_{CO_2}$) for gas-gas collisions and Knudsen diffusion ($D^{kn}_{CO_2}$) for gas-wall collisions [30]:

$$\frac{1}{D^{eff}_{CO_2}} = \frac{\tau_p}{\varepsilon_p}\left(\frac{1}{D^{m}_{CO_2}} + \frac{1}{D^{kn}_{CO_2}}\right). \quad (9)$$

The effective CO_2 diffusivity ($D^{eff}_{CO_2}$) takes into account the catalyst pellet configuration through particle porosity (τ_p), tortuosity (ε_p), average pore diameter (D_{pore}), and molecular

interaction between different species [17]. The molecular diffusion is based on a simplified form of the mixture-averaged diffusion coefficient by Maxwell-Stefan [44]:

$$\frac{1}{D^{m}_{CO_2}} = \sum_{i} \frac{y_i}{D_{ij}} + \frac{y_j}{1 - w_j} \sum_{i} \frac{w_i}{D_{ij}}. \quad (10)$$

Here, $i = H_2$, CH_4 and H_2O and $j = CO_2$. Further, y and w are the mole fraction and the mass fraction, respectively. The binary diffusion coefficients (D_{ij}) are calculated by the equations from Fuller et al. [45]:

$$D_{ij} = \frac{0.00143 \cdot T^{1.75} \cdot \left(\frac{1}{M_i} + \frac{1}{M_j}\right)^{\frac{1}{2}}}{p \cdot \left(\left(\nu_i\right)^{\frac{1}{3}} + \left(\nu_j\right)^{\frac{1}{3}}\right)^{2}}. \quad (11)$$

Here, M_i is the molar mass of component i, and ν_i is the specific diffusion volume of component i (26.9, 7.07, 24.42, and 12.7 for CO_2, H_2, CH_4, and H_2O, respectively) [45]. The Knudsen diffusion is computed as follows, considering only CO_2:

$$D^{kn}_{CO_2} = \frac{D_{pore}}{3} \sqrt{\frac{8 \cdot R \cdot T}{\pi \cdot M_{CO_2}}}. \quad (12)$$

2.4. Numerical Solution Strategy

The balance equations and the correlations for reaction rates and effectiveness factors generate a set of ordinary differential equations (ODEs). The ODEs were solved with MATLAB® R2019a using the *ode15s* function. To solve the ODEs, the initial molar flow of components at the inlet of the reactor is required. A good trade-off between model precision and computational time is achieved by assuming an equidistant step size (representing the cell size along the reactor) of 0.001 m and a relative error tolerance of 10^{-8}. Here, the relative error tolerance refers to the considered significance of digits for the computation of the ODEs. The water removal is implemented numerically by adjusting the molar flow of water to zero at the step where water removal is taking place. The reactor specifications and input values for the model are given in Table 2.

Table 2. Reactor specifications in the PFR model.

Parameter	Unit	Value	Ref.
Temperature range	K	500–600	[41]
Pressure range	bar	1–15	[41]
Catalyst density	kg/m^3	2355.2	[41]
Catalyst void fraction	-	0.4	[17]
H_2/CO_2 ratio	-	4	-
CH_4/CO_2 ratio range	-	0–1.5	-
Inlet CO_2 molar flow rate	mol/s	0.002	-
Tube diameter	m	0.0254	-
Catalyst diameter	m	0.002	[17]
Catalyst pore diameter	nm	10	[17]
Catalyst porosity	-	0.6	[17]
Catalyst tortuosity	-	2	[17]
Ambient temperature	K	298.15	-
Ambient pressure	bar	1.01325	-

3. Methodology

The hypothesis behind removing water at different positions along an FBR is that the CO_2 conversion (and thereby the CH_4 yield) would change by moving the water removal position. In the present study, water is only removed at one point along the reactor, and

the influence of moving the water removal point on the CO_2 conversion is investigated. For the sake of fair comparison, the water produced after the water removal point is removed at the end of the reactor. Before studying the effect of water removal, the reactor length required to reach equilibrium without water removal is identified. At equilibrium, the reaction rate approaches zero, which would require an infinitely long reactor. Here, the equilibrium length ($L_{EQ.1}$) is defined as the point at which 99.9% of the equilibrium conversion is obtained. It is worth mentioning that the equilibrium length of the rector is correlated to the tube diameter. The smaller the tube diameter, the longer is the reactor required to reach the equilibrium composition.

Figure 1a illustrates a tubular FBR, with diameter D and the equilibrium length ($L_{EQ.1}$), in which the entire water removal takes place at the end of the reactor. The case with intermediate water removal along the reactor length is demonstrated in Figure 1b. Conventional directions of material and energy streams are specified in Figure 1. When studying the effect of water removal, reactors lengths (L) shorter than the equilibrium length are examined, varying the water removal point along the reactor. Water is removed at a point z along the reactor. In practice, this assumption can be interpreted as dividing the original reactor with length L into two reactors with lengths of z and L-z, with water removal between the two reactors. In this work, it is assumed that 100% of produced water present at this location is removed. A case with no internal water removal (WR) (i.e., all water removed at the end of the reactor) is given by $z = 0$ or $z = L$. Even though 100% continuous water removal along the reactor is practically impossible, a continuous WR case is considered to account for the theoretical cases of SME and MR. In this case, the water produced in each cell of the reactor model is assumed to be removed in the same cell.

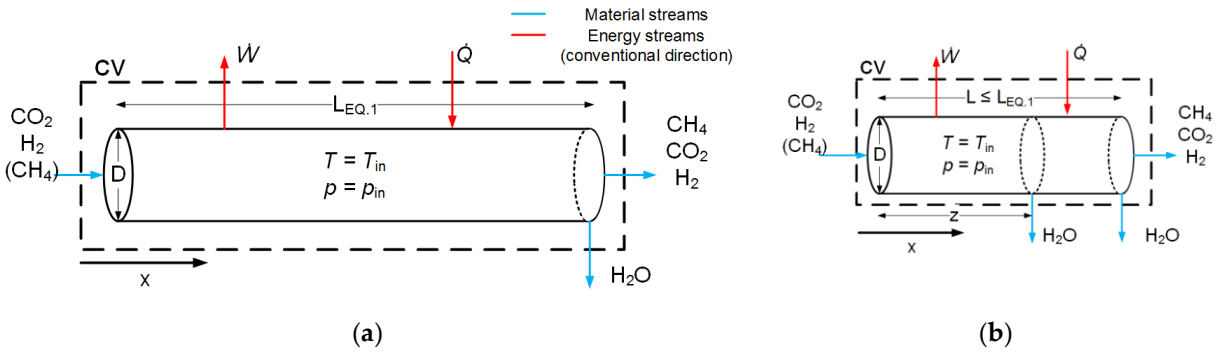

Figure 1. A schematic of a tubular FBR operating under isothermal conditions; (**a**) equilibrium length case, (**b**) intermediate water removal case.

Here, the ratio between H_2 and CO_2 is equal to the stoichiometric ratio of the Sabatier reaction (i.e., 4). Moreover, the ratio between CH_4 and CO_2 (here defined as A) is zero or 1.5, representing pure CO_2 methanation and methanation of a biogas mixture with 60 mol% CH_4 and 40 mol% CO_2, respectively. In the present study, the initial CO_2 molar flow rate is kept constant; accordingly, the initial molar flow rate of H_2 and CH_4 is calculated using the stoichiometric ratio between H_2 and CO_2 and the studied ratio between CH_4 and CO_2, respectively.

The performance of the reactor is evaluated with respect to the CO_2 conversion and the irreversibilities within the reactor. The CO_2 conversion is defined as the change between inlet and outlet CO_2 molar flow in the reactor:

$$X_{CO_2} = \frac{F_{CO_2}^{in} - F_{CO_2}^{out}}{F_{CO_2}^{in}} \quad (13)$$

Since only the Sabatier reaction is considered, the CO_2 conversion will also represent the methane yield from the reactor. In order to compare the effect of water removal for different reactor lengths, the relative conversion improvement (RX_{CO2}) is defined as the

CO_2 conversion improvement for the optimum water removal location compared to the case with no water removal:

$$RX_{CO_2} = \frac{X_{CO_2,@opt} - X_{CO_2,\text{ no WR}}}{X_{CO_2,\text{no WR}}}. \tag{14}$$

As the amount of water removed from the reactor and the CO_2 conversion change with the water removal location, the work requirement for water removal and the irreversibility rate within the rector also change. These changes are investigated using exergy analysis. The total irreversibility rate ($\dot{I}$) within the reactor at steady-state operation, illustrated in Figure 1 is calculated based on changes in exergy of material streams ($\Delta\dot{E}_{x,\text{ streams}}$), the exergy of heat rejected from the reactor ($\dot{E}_x\left(\dot{Q}\right)$) and the work required for water removal within the reactor ($\dot{W}$) according to the methodology described by Kotas [46]:

$$\dot{I} = \Delta\dot{E}_{x,\text{ streams}} + \dot{E}_x\left(\dot{Q}\right) - \dot{W}, \tag{15}$$

$$\Delta\dot{E}_{x,\text{ streams}} = \sum \dot{n}_i \cdot \bar{\varepsilon}_{x,i} - \sum \dot{n}_e \cdot \bar{\varepsilon}_{x,e}, \tag{16}$$

$$\dot{E}_x\left(\dot{Q}\right) = \int \left(1 - \frac{T_0}{T}\right) \cdot \delta\dot{Q}. \tag{17}$$

Here, $\dot{n}_i$ is the molar flow rate and $\bar{\varepsilon}_x$ is the molar exergy, calculated for inlet streams i and outlet streams e. Further, $\dot{Q}$ is the heat flow transferred to the reactor at reactor temperature T and $\dot{W}$ is the power delivered from the reactor. The subscript "0" denotes environment state (here T_0 = 298.15 K, p_0 = 1 atm = 1.01325 bar). In this study, it is assumed that water removal takes place in a reversible process; hence, $\dot{W}$ represents the minimum work required for water removal.

The molar exergy of material streams can be decomposed into physical exergy ($\bar{\varepsilon}_x^{phy}$) and chemical exergy ($\bar{\varepsilon}_x^{chem}$):

$$\bar{\varepsilon}_x = \bar{\varepsilon}_x^{phy} + \bar{\varepsilon}_x^{chem}. \tag{18}$$

By neglecting kinetic and potential energy effects, $\bar{\varepsilon}_x^{phy}$ can be expressed as

$$\bar{\varepsilon}_x^{phy} = \left(\bar{h} - \bar{h}_0\right) - T_0 \cdot (\bar{s} - \bar{s}_0). \tag{19}$$

Based on ideal gas and ideal mixture assumptions, the molar enthalpy and entropy of the mixtures can be calculated as

$$\left(\bar{h} - \bar{h}_0\right) = \sum y_i \cdot \left(\bar{h}_i(T) - \bar{h}_i(T_0)\right), \tag{20}$$

$$(\bar{s} - \bar{s}_0) = \sum y_i \cdot (\bar{s}_i(T, p_i) - \bar{s}_i(T_0, p_{0,i})). \tag{21}$$

Here, y_i is the molar fraction of component i in the mixture, while $\bar{h}$ and $\bar{s}$ refer to the molar enthalpy and entropy of the material stream, respectively. The chemical exergy of an ideal mixture can be calculated as

$$\bar{\varepsilon}_x^{chem} = \sum y_i \cdot \bar{\varepsilon}_{x,i}^{std} + T_0 \cdot \bar{R} \cdot \sum y_i \cdot \ln y_i. \tag{22}$$

The standard chemical exergy of component i in the mixture ($\bar{\varepsilon}_x^{chem}$) is obtained from the reference tables provided by Kotas [46]. Further, $\bar{R}$ is the universal gas constant.

4. Results

4.1. Conversion

According to thermodynamic principles, operating the reactor at a lower temperature and higher pressure is favorable for improving the CO_2 conversion due to the highly

exothermic nature of the Sabatier reaction and the volume reduction after conversion. Figure 2 illustrates the CO_2 conversion within the FBR operating under different conditions when reaction (1) reaches equilibrium. As is expected, higher CO_2 conversion is obtained by increasing the operating pressure and lowering the reactor temperature. Moreover, additional CH_4 in the inlet gas mixture (i.e., cases with A = 1.5) results in a reduction of the CO_2 conversion. Since CH_4 is one of the products in the reaction, the presence of CH_4 in the feed shifts the equilibrium composition towards the reactant side, leading to reduced CO_2 conversion.

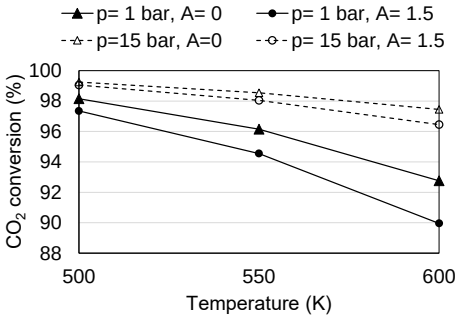

Figure 2. CO_2 conversion at equilibrium composition as a function of operating temperature, pressure, and inlet gas composition (CH_4/CO_2 ratio (A)).

Figure 3 demonstrates the influence of water removal on the CO_2 conversion and reaction rate along a reactor that is operating at 600 K and 1 bar. In Figure 3, the solid red line (EQ.1) illustrates the point at which the reaction is assumed to have reached equilibrium (99.9% of the CO_2 conversion at equilibrium). The dotted red line (EQ.2) illustrates the point at which the reaction reaches a new equilibrium if all produced water is removed at EQ.1. The solid black line ("No WR") illustrates a case with no water removal along the reactor, while the black dotted lines represent cases with water removal at different points in the reactor. Further, the solid blue line demonstrates a case where water is removed continuously along the reactor. In all cases, the reactor is long enough to reach equilibrium after water removal. It is worth mentioning that the cases with no water removal and continuous water removal define the limiting cases with minimum and maximum CO_2 conversion, respectively.

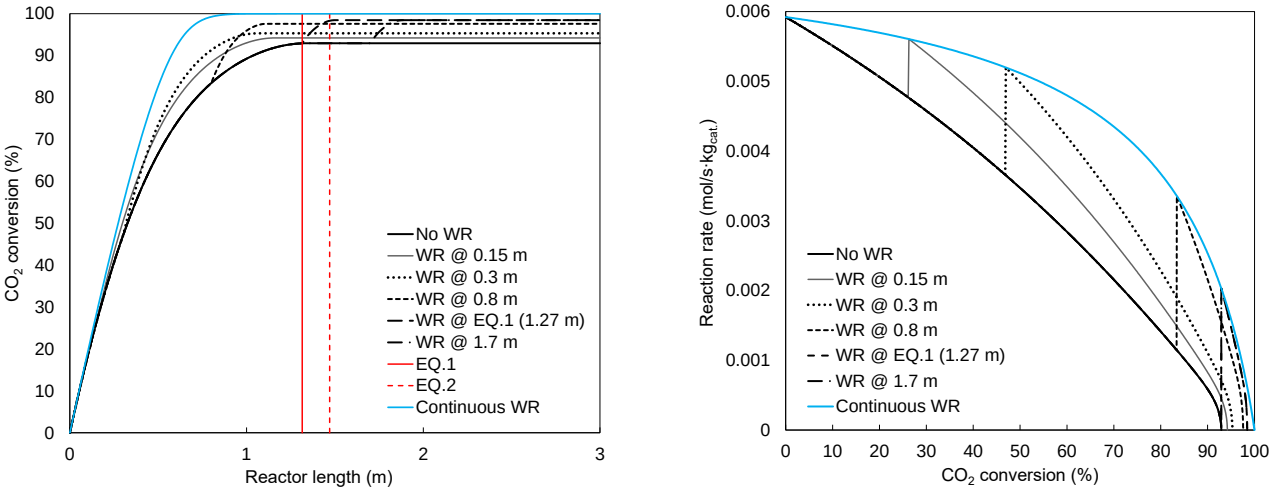

Figure 3. Effect of water removal along a reactor length operating at T = 600 K, p = 1 bar and A = 0 on (**a**) CO_2 conversion and (**b**) reaction rate. Here, EQ.1 and EQ.2 denote the first and second equilibrium lengths. Notice that the lines for water removal at EQ.1 and 1.7 m are the same in (**b**).

As can be seen in Figure 3a, removing water from the reactor increases the CO_2 conversion compared to the case with no water removal. As expected, maximum CO_2 conversion is obtained when the water is removed after reaching the first equilibrium. It should be noticed that most of the conversion takes place before reaching the first equilibrium and that the length extension required to reach the second equilibrium point is smaller than the length required to reach the first equilibrium. This can be also seen in Figure 3b, where the reaction rate along the reactor is illustrated. It can be observed that water removal causes an abrupt increase in the reaction rate, increasing the average reaction rate compared to the case with no water removal. When the reaction reaches the first equilibrium, no further conversion takes place due to zero reaction rate. No matter where water is removed after reaching the first equilibrium length, the reaction rate reaches an identical maximum value and then approaches zero where the second equilibrium is obtained (see the identical lines for water removal at the first equilibrium and 1.7 m in Figure 3b). If the water removal point is located before reaching equilibrium, the total CO_2 conversion is reduced. However, the reaction rate is higher, and the conversion can be improved if the reactor is not long enough to reach equilibrium.

Figure 4 illustrates the CO_2 conversion improvement and relative length extension required to obtain maximum CO_2 conversion under different operating conditions. The length required to reach the first equilibrium point depends on the kinetics of the reaction. Operating the CO_2 methanation reactor at a higher pressure and temperature increases the reaction rate, thereby reducing the length required to reach equilibrium. Moreover, the presence of CH_4 in the inlet gas mixture reduces the reaction rate, hence increasing the length required to reach equilibrium. These trends also apply to the relative length extension required to reach the second equilibrium after removing water.

As can be observed in Figure 4, the relative conversion improvement is higher under conditions where CO_2 conversion is limited due to the thermodynamic equilibrium (i.e., low pressure, high temperature, and CH_4 in the feed). This suggests that the water removal is of more significance when the final CO_2 conversion at the first equilibrium length is lower. For instance, the highest CO_2 conversion improvement of approximately 8% is achieved for the case with the lowest conversion at the first equilibrium point (corresponding to the situation in Figure 2, i.e., at p = 1 bar, T = 600 K and A = 1.5).

As mentioned earlier in this section, both the CO_2 conversion and the conversion rate changes when moving the point of the water removal. This becomes important when the reactor is not long enough to reach equilibrium. The effect of the water removal location on the CO_2 conversion for a reactor with a length equal to 50% of the first equilibrium length ($L_{EQ.1}$) is illustrated in Figure 5. It should be noted that the results for water removal at either the inlet or the outlet of the reactor are the same since no water removal takes place along the reactor in both cases. As can be seen in Figure 5, there is an optimal location for the water removal at which the CO_2 conversion is maximized. Corresponding to Figure 3b, the optimal point for water removal should be where the average reaction rate is highest. The reaction rate is reduced as the number of products increases. After removing water, the driving force for the reaction, and thereby the reaction rate, increases. The later the water removal, the higher the conversion will be at equilibrium. However, if the water is removed too late, there will not be enough length left to take advantage of the increased reaction rate.

Figure 6 illustrates the effect of operating conditions on the optimum water removal location for different lengths of the reactor. The optimal location is here defined as the water removal point that gives the maximum CO_2 conversion for a given reactor length. However, the optimal point is only refined to a resolution of 0.1 in z/L. As can be observed in Figure 6, for a given operating pressure, the optimum water removal location is independent of the reactor temperature. The shorter the length of the reactor, the earlier the water removal must take place to maximize the conversion. At higher pressure, the results indicate that the optimal point of water removal is at a higher relative length of z/L.

As can be observed in Figure 3b, the reaction rate drops faster after removing the water. To overcome this limitation, the optimal value for the relative point for water removal will not be smaller than 0.5 even in short reactors. For the cases where CH_4 is present in the inlet gas mixture, the optimal value for the relative length of z/L is generally smaller. With A = 1.5 and low pressure, the optimal point is the same for all relative reactor lengths below 0.75. Corresponding to Figure 4, the presence of CH_4 in the feed gas reduces the reaction rate, thereby increasing the length required to reach equilibrium.

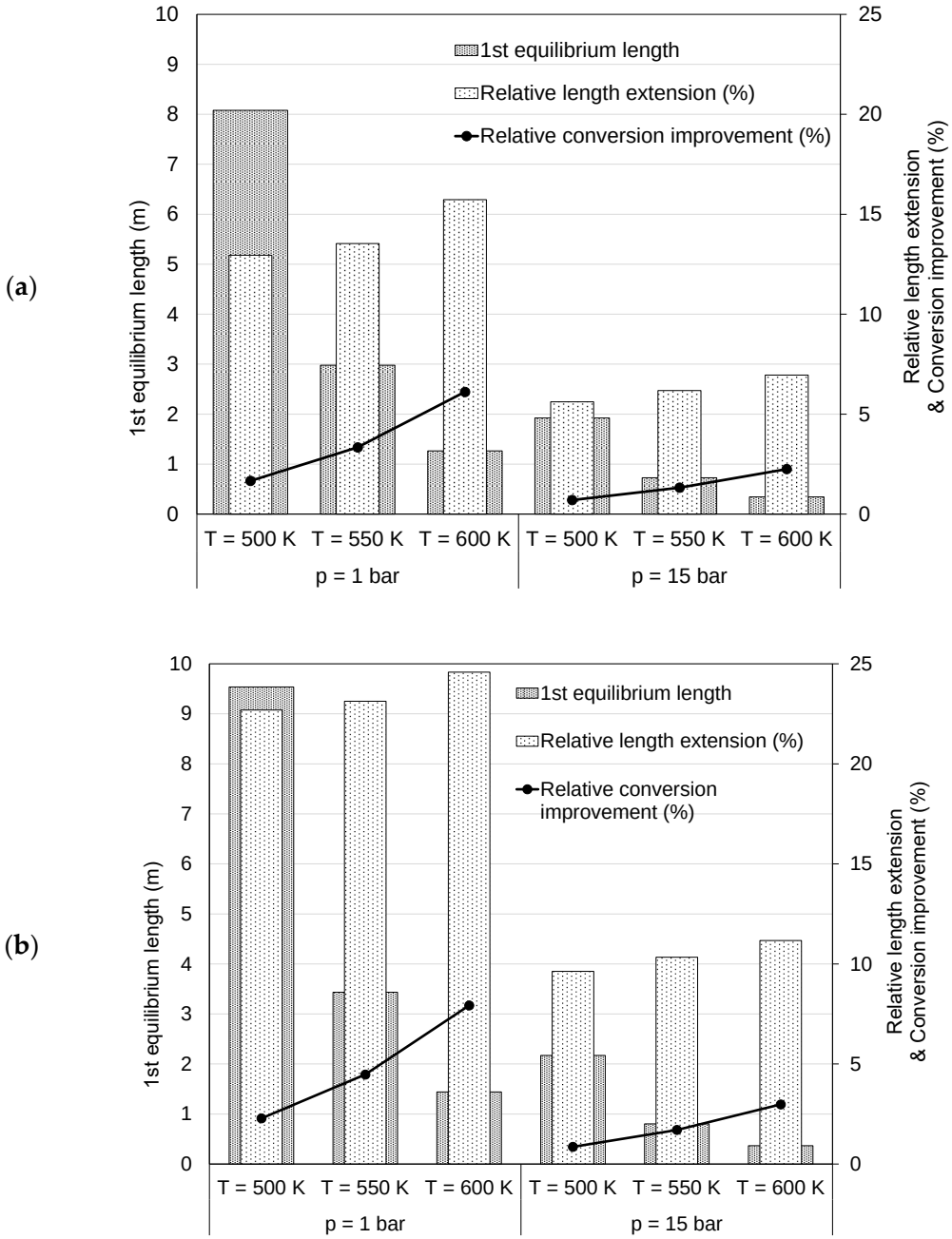

Figure 4. CO_2 conversion improvement and relative length extension required to the 2nd equilibrium under different operating conditions for (**a**) A = 0 and (**b**) A = 1.5.

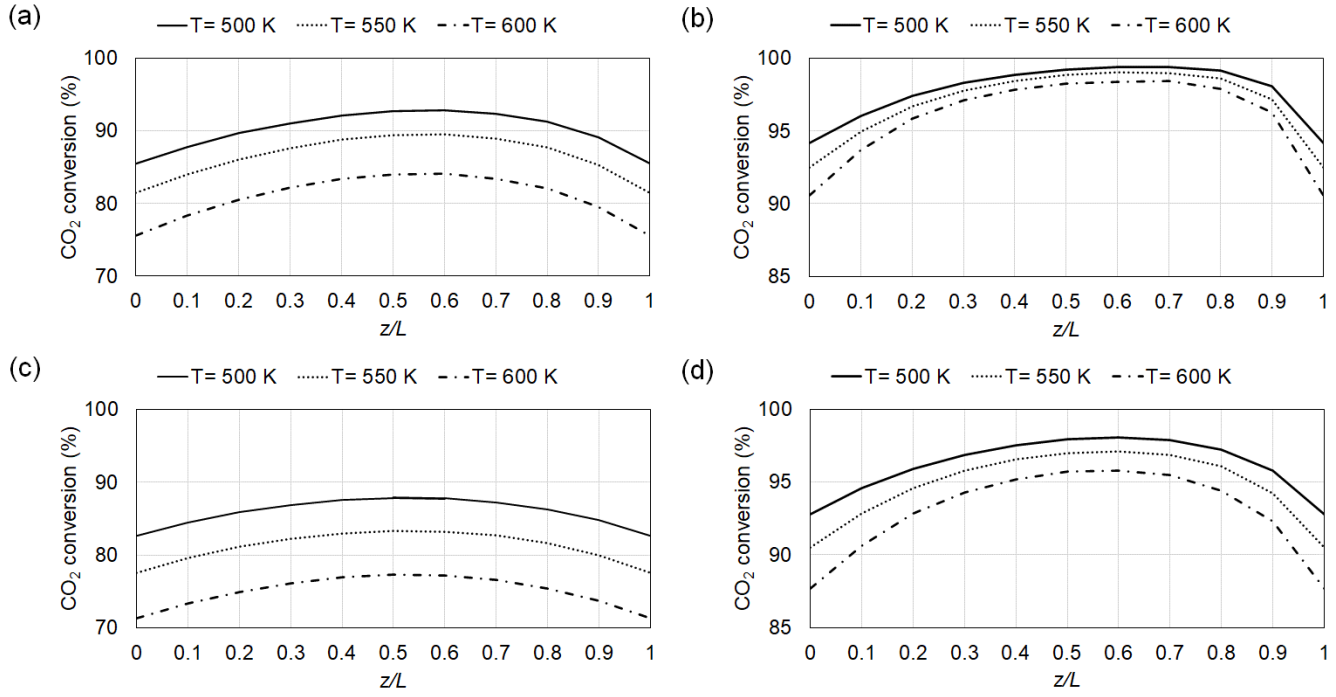

Figure 5. Effect of the water removal location on the CO_2 conversion for a reactor with $L/L_{EQ.1} = 0.5$ operating under different temperature, pressure, and CH_4/CO_2 ratios (A). (**a**) $p = 1$ bar and $A = 0$, (**b**) $p = 15$ bar and $A = 0$, (**c**) $p = 1$ bar and $A = 1.5$, (**d**) $p = 15$ bar and $A = 1.5$.

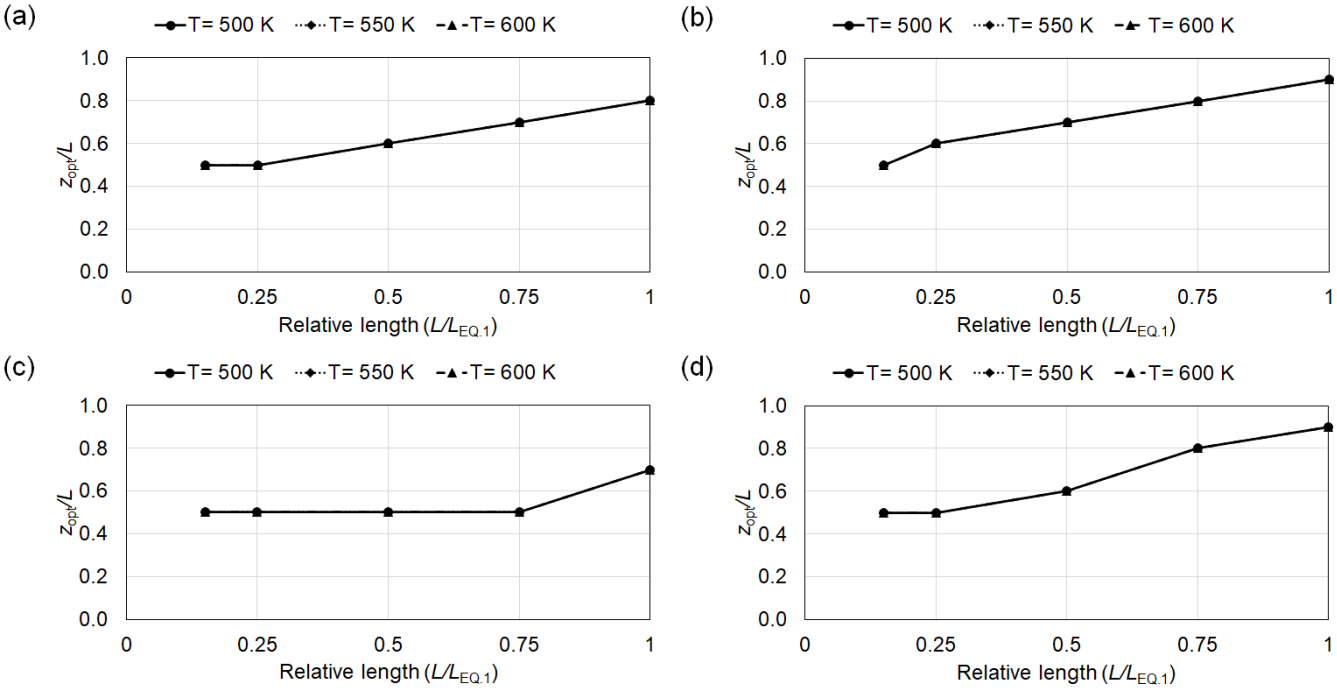

Figure 6. Effect of operating conditions on the optimum water removal point for different lengths of the reactor. (**a**) $p = 1$ bar and $A = 0$, (**b**) $p = 15$ bar and $A = 0$, (**c**) $p = 1$ bar and $A = 1.5$, (**d**) $p = 15$ bar and $A = 1.5$.

The relative conversion improvement for different reactor lengths under different operating conditions is demonstrated in Figure 7. The water removal leads to larger CO_2 conversion improvement when the length of the reactor is shorter than the first equilibrium length. At low operating pressure, the strongest effect on the relative conversion

improvement due to water removal is seen at the relative length ($L/L_{EQ.1}$) of 0.5, whereas the strongest effect is observed at the relative length ($L/L_{EQ.1}$) of 0.25 at higher operating pressure. For short reactors, the reaction will not reach equilibrium. Nonetheless, an effort to increase the average reaction rate is favorable as this gives a higher conversion. The largest relative conversion improvement due to water removal is achieved in the case without CH_4 in the inlet gas mixture, operating at high pressure and high temperature. Referring to Figure 3b, it was observed that water removal boosted the average reaction rate, and the new equilibrium condition would be obtained earlier. Moreover, increasing the operating temperature and pressure improves the reaction rate and this will be amplified by removing water in a short reactor.

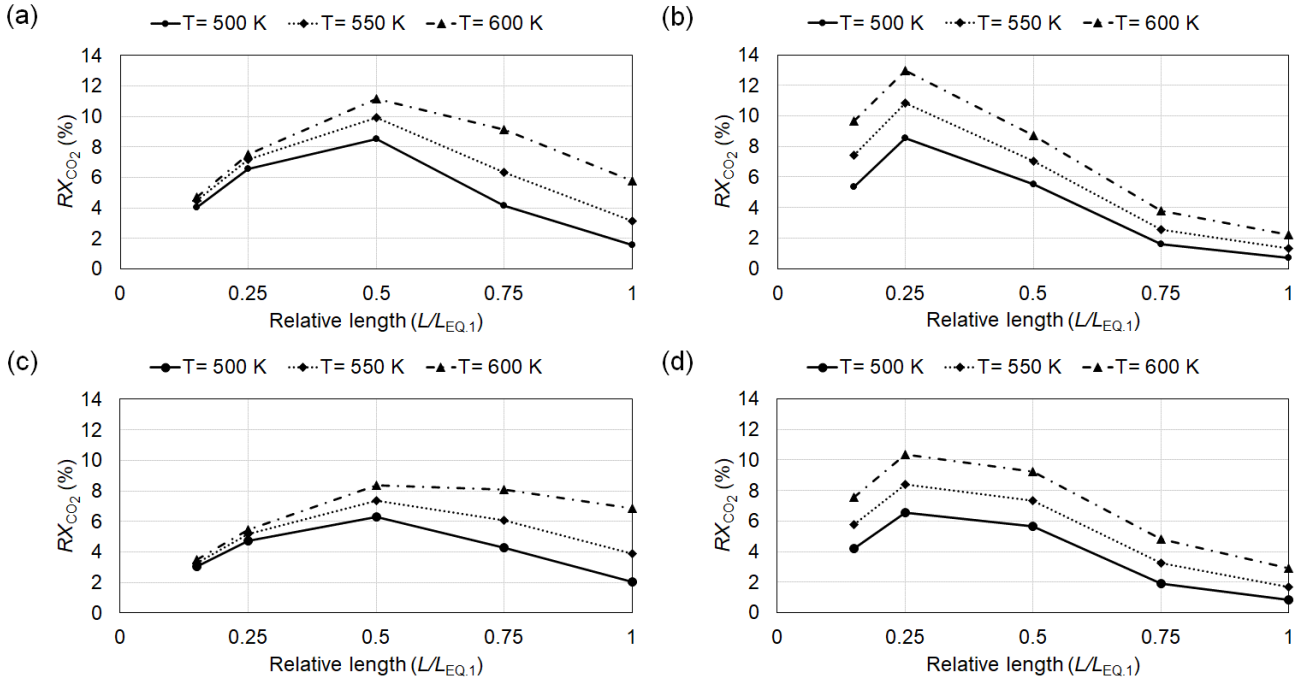

Figure 7. Relative conversion improvement for different lengths of the reactor under different operating conditions. (**a**) p = 1 bar and A = 0, (**b**) p = 15 bar and A = 0, (**c**) p = 1 bar and A = 1.5, (**d**) p = 15 bar and A = 1.5.

4.2. Irreversibility

The present section focuses on assessing the performance of the methanation reactor in terms of energy efficiency. This is realized by analyzing the irreversibility rate of a reactor with or without intermediate water removal. In cases without intermediate water removal, the analysis is presented for the final composition at the end of a reactor sufficiently long to reach equilibrium.

Figure 8 illustrates the specific irreversibility (i.e., the ratio between the total irreversibility rate and the amount of CH_4 produced) within a reactor operating under different conditions for cases without intermediate water removal. As can be observed in Figure 8, operating at lower pressure and higher temperature decreases the specific irreversibility within the reactor. Also, the existence of CH_4 in the inlet gas mixture reduces the specific irreversibility within the reactor. Contrarily, results in Figure 2 illustrated that the CO_2 conversion decreased if the reactor operated at low pressure, high temperature, and in the presence of CH_4 in the inlet gas mixture. These two perspectives suggest that the reactor design should reflect a compromise between CO_2 conversion and irreversibility. From a reversibility point of view, to reduce the thermodynamic losses within the reactor the reaction should follow a path where the magnitude of the reaction driving forces along the reactor approaches zero (i.e., theoretically proceeding the chemical reaction infinitesimally close to equilibrium). Here, in cases with no intermediate water removal, the final CO_2

conversion and the specific irreversibility are only influenced by the fixed operating conditions. Therefore, the degrees of freedom to manipulate the driving forces, and thereby the extent of reaction, are limited.

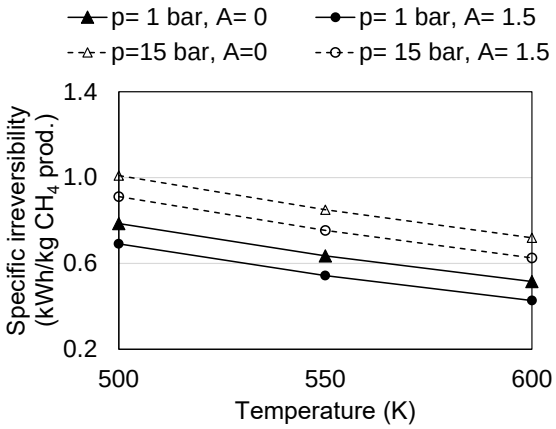

Figure 8. Specific irreversibility within a reactor operating under different conditions with no intermediate water removal.

Figure 9 illustrates the specific work required for water removal, the specific exergy of heat rejected from the reactor, and the change in specific exergy of material streams for a reactor operating under different conditions. As can be seen in Figure 9a, the work required to remove water from the reactor increases with increasing temperature. The presence of CH_4 in the inlet gas mixture also leads to an increase in the work requirement for water removal, as part of the work would be used to separate water from the additional CH_4 in the gas mixture. However, an increase in operating pressure decreases the work required to remove water. Figure 9b illustrates that the exergy of heat extracted from the reactor is independent of the operating pressure and the inlet gas composition. Running the reactor at higher temperature results in increased available exergy of heat, which can be utilized in the overall process design when potential process integration options are considered, contributing to reduced total irreversibility rate at higher temperatures. As can be observed in Figure 9c, operating the reactor at higher temperature and pressure enables extracting more exergy from the material streams, which is also observed in the CO_2 conversion in Figure 2. For a given temperature and pressure, additional CH_4 in the inlet gas mixture leads to a reduction in the exergy extraction from the material streams. The results in Figure 9c are reflected in the specific irreversibility presented in Figure 8.

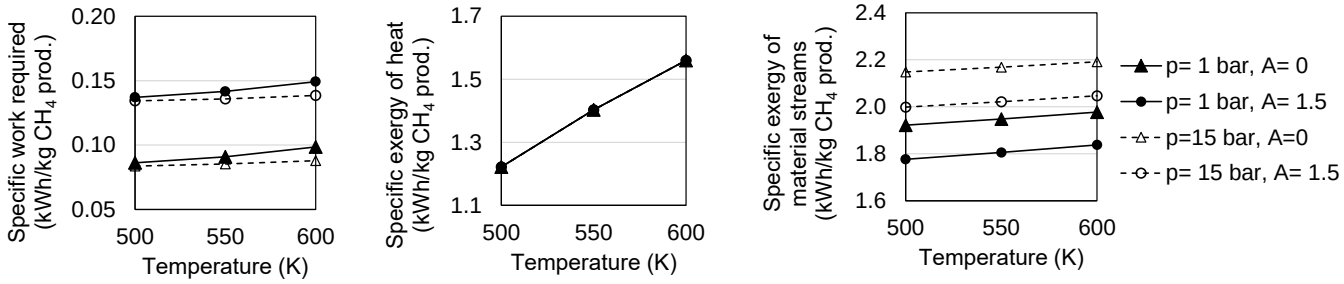

Figure 9. Contribution of the exergy terms for a reactor at the equilibrium operating under different conditions (**a**) specific work ($\dot{W}/\dot{m}_{CH_4\ prod.}$) (**b**) specific exergy of heat ($\dot{E}_x\left(\dot{Q}\right)/\dot{m}_{CH_4\ prod.}$) and (**c**) specific exergy change for material streams ($\Delta\dot{E}_{x,streams}/\dot{m}_{CH_4\ prod.}$).

Here, the effect of the intermediate water removal location on the irreversibility rate within the reactor is studied. In cases with intermediate water removal, the water produced after the removal point is removed at the end of the reactor, to provide a fair comparison between the different cases. Figure 10 demonstrates the effect of the water removal location on the accumulated irreversibility rate and specific irreversibility along a reactor operating at T = 600 K, p = 1 bar, and A = 0. It is worth mentioning that the results in Figure 10 are considered for the same cases as in Figure 3. Here, the specific irreversibility refers to the ratio between the irreversibility rate and the amount of produced CH_4 in each cell of the reactor. As can be observed in Figure 10a, compared to the case with no intermediate water removal, removing water at the intermediate point increases the total irreversibility rate within the reactor. It can be observed that the increase in the irreversibility rate reaches a maximum value when the water is removed at a certain intermediate point. Continuous water removal yields the highest irreversibility rate within the reactor (solid blue line).

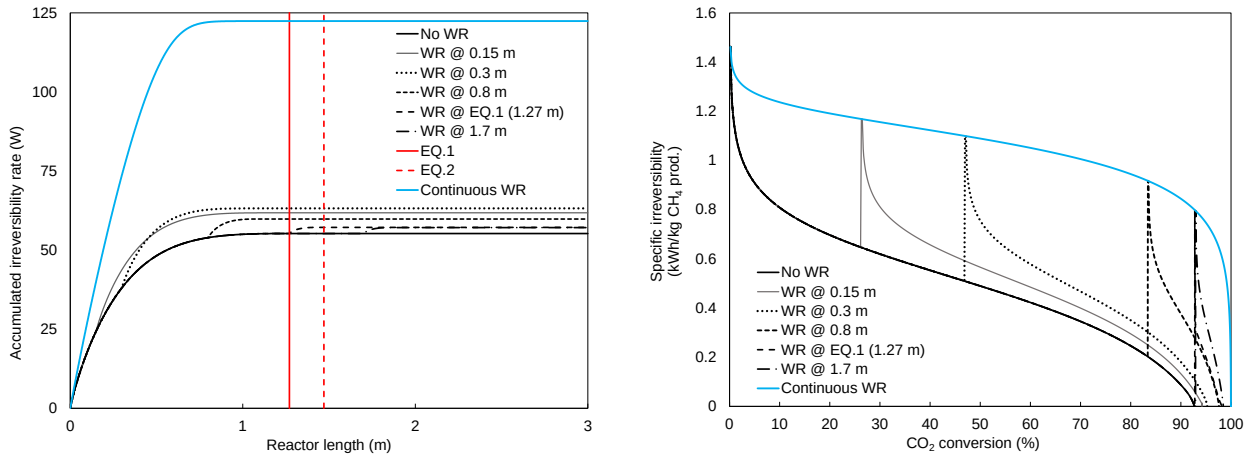

(**a**) (**b**)

Figure 10. Effect of water removal location on (**a**) accumulated irreversibility rate and (**b**) specific irreversibility for a reactor operating at T = 600 K, p = 1 bar, and A = 0. Notice that the lines of water removal at EQ.1 and 1.7 m are the same in (**b**).

In Figure 10b, the intermediate water removal point is observed as a sudden jump in the curves, which leads to higher average specific irreversibility within the reactor. The areas below the curves in Figure 10b indicate the total irreversibility rate within the reactor. As can be observed in Figure 10b, the CO_2 conversion improvement is accompanied by a smaller increase in the irreversibility rate when the intermediate water removal point moves towards the end of the rector. A smaller increase in the average specific irreversibility can be seen when the water is removed after the first equilibrium length (i.e., where the specific irreversibility becomes zero since no reaction occurs in the reactor). In this particular case study, with no length limitation and fixed operating conditions, the results of the irreversibility analysis suggest that water should be removed when the reaction reaches equilibrium.

Results for the specific irreversibility within a reactor operating at T = 600 K, p = 1 bar, and A = 0 are tabulated in Table 3 when the water is removed at different intermediate locations. An increase in the CO_2 conversion due to moving the water removal point towards the end of the reactor length is accompanied by a decrease in the change of specific exergy of material streams. Since the temperature and heat of the reaction are constant, the specific exergy of heat remains constant when moving the water removal point. When the water is removed after reaching the first equilibrium, a smaller total specific irreversibility is obtained compared to the case with no intermediate water removal. This is because the average specific irreversibility before the removal point would be higher than the obtained peak value for the specific irreversibility due to the water removal. Therefore, the amount of total specific irreversibility would reduce.

Table 3. Summarized results for the effect of water removal location (z) along a reactor operating at T = 600 K, p = 1 bar, and A = 0, considering an FBR with a length of 3 m.

x (m)	X_{CO2} (%)	$\Delta \dot{E}_{x,\ streams} / \dot{m}_{CH_4\ prod.}$ (kWh/kg CH_4 Prod.)	$\dot{E}_x\left(\dot{Q}\right) / \dot{m}_{CH_4\ prod.}$ (kWh/kg CH_4 Prod.)	$\dot{W} / \dot{m}_{CH_4\ prod.}$ (kWh/kg CH_4 Prod.)	$\dot{I} / \dot{m}_{CH_4\ prod.}$ (kWh/kg CH_4 Prod.)
No WR	92.9	1.976	1.560	0.098	0.514
0.15	94.2	1.972	1.560	0.155	0.567
0.3	95.3	1.968	1.560	0.166	0.574
0.8	97.6	1.958	1.560	0.132	0.530
1.27 *	98.4	1.954	1.560	0.109	0.502
1.7	98.4	1.954	1.560	0.109	0.502
Continuous WR	100.0	1.942	1.560	0.678	1.060

* The intermediate water removal occurs at the first equilibrium length (EQ.1).

As it is assumed that the water separation is achieved through a reversible process, no additional irreversibility caused by the water removal process is expected. As can be seen in Table 3, in comparison with no water removal case, the increase in the total specific irreversibility due to water removal is accompanied by additional reversible specific work. This suggests that considering the specific work required for water removal from a reactor operating at fixed conditions can be an alternative approach to investigate how the water removal location would influence the irreversibility rate.

The minimum work comprises the work required for water removal at the intermediate location and the end of the reactor. The effect of the water removal location on the amount of removed water and the specific work is demonstrated in Figure 11a,b, respectively, for a reactor operating at T = 600 K, p = 1 bar, and A = 0. By moving the water removal point from the inlet of the reactor towards the outlet of the reactor, the amount of removed water at the intermediate location increases, reaching a maximum amount when the intermediate water removal occurs at the first equilibrium length. As illustrated in Figure 11, the amount of water removed at the intermediate point would not necessarily reflect the required specific work at the intermediate point. The specific work at the intermediate point decreases as the intermediate point moves towards the end of the reactor, reaching a constant value when equilibrium is obtained. Moreover, the larger the amount of water removed at the intermediate point, the higher the specific work required at the end of the reactor to separate the additional produced water after the water removal point. The work required for water removal depends on the composition of the gas mixture, and the specific work requirement for water removal increases as the water fraction reduces.

As discussed earlier, removing water from the reactor increases the average reaction rate. Hence the same conversion can be obtained in a shorter reactor. However, the increase in the average reaction rate would cause an unavoidable increase in irreversibility when the operating conditions for the reaction are fixed. Here, the aim is to investigate how the water removal location can influence the irreversibility rate within reactors shorter than the required equilibrium length (similar to the case studies in Section 4.1.). The effect of the water removal point on the specific irreversibility for different relative reactor lengths operating at T = 600 K, p = 1 bar, and A = 0 is illustrated in Figure 12. Further, Figure 13 demonstrates the specific work required for water removal, the specific exergy of heat rejected from the reactor, and the changes in specific exergy of material streams for the cases presented in Figure 12.

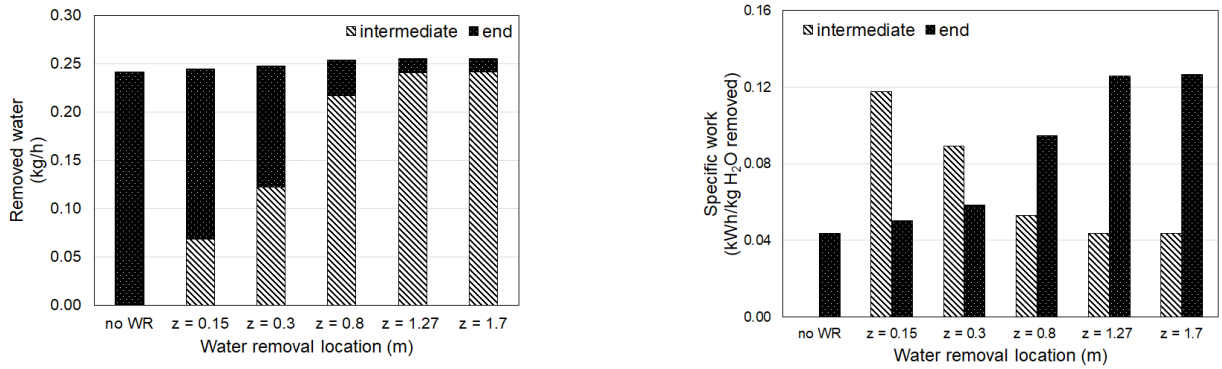

(**a**) (**b**)

Figure 11. The effect of water removal location on (**a**) the amount of removed and (**b**) the specific water removal work at the intermediate point and the end of a reactor operating at T = 600 K, p = 1 bar, and A = 0 with a length of 3 m.

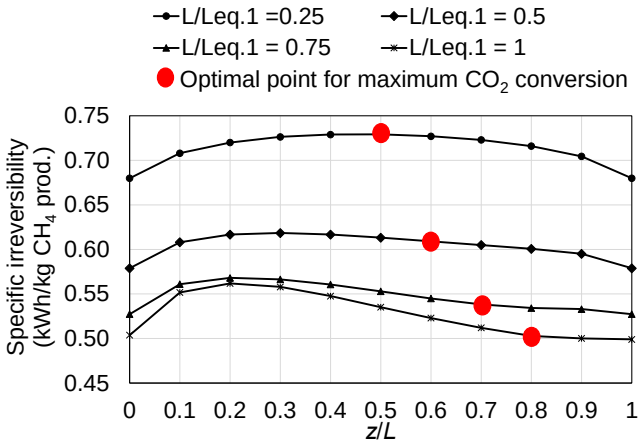

Figure 12. Effect of water removal point on the specific irreversibility for different reactor lengths operating at T = 600 K, p = 1 bar, and A = 0.

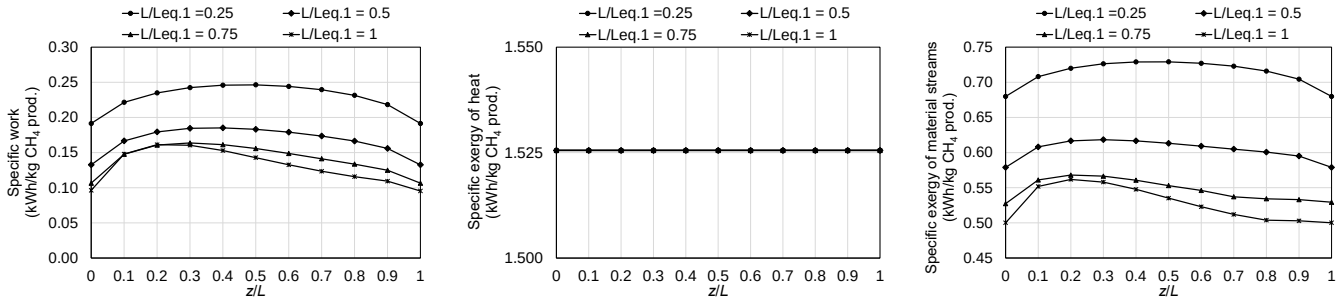

(**a**) (**b**) (**c**)

Figure 13. Effect of water removal point on (**a**) the specific work, (**b**) the specific exergy of heat, and (**c**) the specific exergy of material streams for different reactor lengths operating at T = 600 K, p = 1 bar, and A = 0.

As can be observed in Figure 12, for a short reactor (e.g., $L/L_{EQ.1}$ = 0.25), the highest specific irreversibility is obtained when the water removal occurs in the middle of the reactor. This coincides with where the maximum CO_2 conversion is obtained (at z/L = 0.5). As the reactor length is increased, the optimal water removal point is shifted towards the outlet of the reactor, while the largest irreversibilities are observed for water removal points closer to the inlet of the reactor. Moreover, for the optimal water removal point (in terms of conversion), the increase in specific irreversibility compared to the case with no water

removal is reduced. When the reactor length is equal to the equilibrium length EQ.1, there is only a small penalty compared to the irreversibilities in the case with no water removal. This can be explained by the direct effect of the water removal location on the average specific irreversibility and average reaction rate. As discussed earlier, the benefits from reduced specific irreversibility for longer reactors at the optimal water removal point are reflected in the required specific work and the change in specific exergy of the streams (see Figure 13).

5. Remarks

The present study illustrates that considering intermediate water removal increases the average reaction rate within the reactor and, as a result, increases the CO_2 conversion and the irreversibility rate within a reactor operating at fixed conditions. As mentioned earlier, obtaining a fixed isothermal condition for a highly activated catalytic reaction is a challenging task in practice. Besides, the fixed operating conditions limit the degrees of freedom to manipulate the driving forces within the reactor to obtain an energy-efficient reactor design. Therefore, an extended study should consider adding more complexity to the reactor model, e.g., non-isothermal operating modes.

In the present study, the examination of removing water at an intermediate point demonstrated the potential possibility of manipulation of the average reaction rate through changing driving forces leading to different irreversibility rates. To avoid a significant increase in the reaction rate at the water removal point, and thereby a significant jump in the specific irreversibility, partial water removal (instead of complete water removal at the intermediate point) or water removal at several points can be considered as alternatives. It is worth mentioning that partial water removal results in longer reactors while the effect of multiple removal points will be reduced reactor length Nonetheless, the length of the reactor might not be an important factor if an energy-efficient reactor with a high CO_2 conversion is guaranteed.

The intermediate water removal concept can also be accompanied by a partial feeding strategy of reactants along the reactor. On the one hand, water removal increases the average reaction rate, while on the other hand, a limited concentration of the reactants would reduce the average reaction rate. This can aid in controlling the reaction rate within the reactor. Considering a combination of water removal and partial feeding of the reactants can lead to efficient heat management within the reactor, at which high CO_2 conversion can be obtained even though the irreversibility rate is low. It is observed that the work required for removing water at an intermediate location could be used as an alternative approach to investigate the irreversibility rate within the reactor. However, it should be noted that the actual work for water removal will be higher than what is presented here, as, in the present study, the produced water was removed in reversible processes.

6. Conclusions

A comprehensive thermodynamic study was performed in order to investigate the effect of water removal on the CO_2 conversion and the irreversibility in an isothermal fixed bed methanation reactor. A one-dimensional pseudo-homogenous model was applied for the reactor, considering the kinetics of the Sabatier reaction. An effectiveness factor was used to consider the intra-particle mass and heat transport limitations between the two phases. At one intermediate point in the reactor, all the water produced up until that point was is removed, assuming a reversible process.

With respect to the CO_2 conversion, for short reactors, the optimal water removal point was located in the middle of the reactor. As the length of the reactor approached the length required to reach equilibrium, the water removal point resulting in the highest CO_2 conversion moved closer to the end. The location of the optimal removal point was found to be independent of the operating temperature, while the presence of CH_4 in the feed gas resulted in moving the optimal water removal point upstream.

With respect to the irreversibility within the reactor, for a short reactor, it was observed that the water removal point that gave the highest CO_2 conversion in the middle of the reactor also provided the largest irreversibility rate. For a longer reactor (i.e., reactor lengths close to the required equilibrium length), the improvement in the CO_2 conversion was accompanied by a smaller penalty in the irreversibilities compared to the case with no water removal.

The results illustrate that the length of the reactor is essential to the optimal water removal point. Further, it is demonstrated that the reactor length should not necessarily be close to the equilibrium length when the water removal takes place to obtain the best performance; the additional gains in terms of both the CO_2 conversion and the irreversibilities are not significant.

Possible conceptual ideas such as partial water removal and partial reactant feeding are suggested for future studies to develop an energy-efficient reactor. These ideas are based on manipulating the reaction rate within the reactor to control the driving forces along the reactor. The proposed model should be examined using process simulators, and for cases operating under non-isothermal conditions in future work. In this context, additional concerns such as runaway temperature limitations should be considered.

Author Contributions: Conceptualization, S.E.H. and K.M.L.; methodology, S.E.H.; software, S.E.H.; validation, S.E.H., M.H. and B.A.; formal analysis, S.E.H.; investigation, S.E.H.; resources, S.E.H. and K.M.L.; data curation, S.E.H.; writing—original draft preparation, S.E.H.; writing—review and editing, K.M.L., S.K.S., M.H. and B.A.; supervision, B.A.; project administration, B.A. All authors have read and agreed to the published version of the manuscript.

Funding: This research received no external funding.

Institutional Review Board Statement: Not applicable.

Informed Consent Statement: Not applicable.

Data Availability Statement: Data sharing not applicable.

Acknowledgments: The authors acknowledge the financial support from the Norwegian University of Science and Technology (NTNU) through the Strategic Research Program ENERSENSE.

Conflicts of Interest: The authors declare no conflict of interest.

References

1. He, W.; Abbas, Q.; Alharthi, M.; Mohsin, M.; Hanif, I.; Vo, X.V.; Taghizadeh-Hesary, F. Integration of renewable hydrogen in light-duty vehicle: Nexus between energy security and low carbon emission resources. *Int. J. Hydrogen Energy* **2020**, *45*, 27958–27968. [CrossRef]
2. Pao, H.T.; Tsai, C.M. CO_2 emissions, energy consumption and economic growth in BRIC countries. *Energy Policy* **2010**, *38*, 7850–7860. [CrossRef]
3. Balsalobre-Lorente, D.; Shahbaz, M.; Roubaud, D.; Farhani, S. How economic growth, renewable electricity and natural resources contribute to CO_2 emissions? *Energy Policy* **2018**, *113*, 356–367. [CrossRef]
4. Sinsel, S.R.; Riemke, R.L.; Hoffmann, V.H. Challenges and solution technologies for the integration of variable renewable energy sources—A review. *Renew. Energy* **2020**, *145*, 2271–2285. [CrossRef]
5. Gallo, A.B.; Simões-Moreira, J.R.; Costa, H.K.M.; Santos, M.M.; Moutinho dos Santos, E. Energy storage in the energy transition context: A technology review. *Renew. Sustain. Energy Rev.* **2016**, *65*, 800–822. [CrossRef]
6. Parra, D.; Valverde, L.; Pino, F.J.; Patel, M.K. A review on the role, cost and value of hydrogen energy systems for deep decarbonization. *Renew. Sustain. Energy Rev.* **2019**, *101*, 279–294. [CrossRef]
7. Ghaib, K.; Ben-Fares, F.Z. Power-to-Methane: A state-of-the-art review. *Renewable Sustainable Energy Rev.* **2018**, *81*, 433–446. [CrossRef]
8. Uebbing, J.; Rikho-Struckmann, L.K.; Sunmacher, K. Exergetic assessment of CO_2 methanation processes for the chemical storage of renewable energies. *Appl. Energy* **2019**, *233*, 271–282. [CrossRef]
9. Massa, F.; Coppola, A.; Scala, F. A thermodynamic study of sorption-enhanced CO_2 methanation at low pressure. *J. CO_2 Util.* **2020**, *35*, 176–184. [CrossRef]
10. Mazza, A.; Bompard, E.; Chicco, G. Applications of power to gas technologies in emerging electrical systems. *Renew. Sustain. Energy Rev.* **2018**, *92*, 794–806. [CrossRef]
11. Sabatier, P.; Senderens, J.B. New Synthesis of Methane. *C. R. Hebd. Séances Acad. Sci.* **1902**, *134*, 514–516.

12. Rönsch, S.; Schneider, J.; Matthischke, S.; Schlüter, M.; Götz, M.; Lefebvre, J.; Prabhakaran, P.; Bajhor, S. Review on methanation—From fundamentals to current projects. *Fuel* **2016**, *166*, 276–296. [CrossRef]
13. Ngo, S.I.; Lim, Y.I.; Lee, D.; Go, K.S.; Seo, M.W. Flow behaviors, reaction kinetics, and optimal design of fixed- and fluidized-beds for CO_2 methanation. *Fuel* **2020**, *275*, 117886. [CrossRef]
14. Kao, Y.L.; Lee, P.H.; Tseng, Y.T.; Chien, I.L.; Ward, J.D. Design, control and comparison of fixed-bed methanation reactor systems for the production of substitute natural gas. *J. Taiwan Inst. Chem. Eng.* **2014**, *45*, 2346–2357. [CrossRef]
15. Schlereth, D.; Hinrichsen, O. A fixed-bed reactor modeling study on the methanation of CO_2. *Chem. Eng. Res. Des.* **2014**, *92*, 702–712. [CrossRef]
16. Fache, A.; Marias, F.; Guerré, V.; Palmade, S. Optimization of fixed-bed methanation reactors: Safe and efficient operation under transient and steady-state conditions. *Chem. Eng. Sci.* **2018**, *192*, 1124–1137. [CrossRef]
17. Bremer, J.; Sundmacher, K. Operation range extension via hot-spot control for catalytic CO_2 methanation reactors. *React. Chem. Eng.* **2019**, *4*, 1019–1037. [CrossRef]
18. Zimmermann, R.T.; Bremer, J.; Sundmacher, K. Optimal catalyst particle design for flexible fixed-bed CO_2 methanation reactors. *Chem. Eng. J.* **2020**, *387*, 123704. [CrossRef]
19. Kopyscinski, J.; Schildhauer, T.J.; Biollaz, S.M.A. Methanation in a fluidized bed reactor with high initial CO partial pressure: Part II—Modeling and sensitivity study. *Chem. Eng. Sci.* **2011**, *66*, 1612–1621. [CrossRef]
20. Herce, C.; Cortés, C.; Stendardo, S. Numerical simulation of a bubbling fluidized bed reactor for sorption-enhanced steam methane reforming under industrially relevant conditions: Effect of sorbent (dolomite and CaO-$Ca_{12}Al_{14}O_{33}$) and operational parameters. *Fuel Process. Technol.* **2019**, *186*, 137–148. [CrossRef]
21. Li, J.; Zhou, L.; Li, P.; Zhu, Q.; Jiajian, G.; Gu, F.; Su, F. Enhanced fluidized bed methanation over a Ni/Al_2O_3 catalyst for production of synthetic natural gas. *Chem. Eng. J.* **2013**, *219*, 183–189. [CrossRef]
22. Meng, F.; Li, X.; Li, M.; Cui, X.; Zhong, L. Catalytic performance of CO methanation over La-promoted Ni/Al_2O_3 catalyst in a slurry-bed reactor. *Chem. Eng. J.* **2017**, *313*, 1548–1555. [CrossRef]
23. Lefebvre, J.; Bajohr, S.; Kolb, T. Modeling of the transient behavior of a slurry bubble column reactor for CO_2 methanation, and comparison with a tube bundle reactor. *Renew. Energy* **2020**, *151*, 118–136. [CrossRef]
24. Lefebvre, J.; Götz, M.; Bajohr, S.; Reimert, R.; Kolb, T. Improvement of three-phase methanation reactor performance for steady-state and transient operation. *Fuel Process. Technol.* **2015**, *132*, 83–90. [CrossRef]
25. Engelbrecht, N.; Chiuta, S.; Everson, R.C.; Neomagus, H.W.J.P.; Bessarabov, D.G. Experimentation and CFD modelling of a microchannel reactor for carbon dioxide methanation. *Chem. Eng. J.* **2017**, *313*, 847–857. [CrossRef]
26. Mathieu-Potvin, F.; Gosselin, L. Threshold length for maximal reaction rate in catalytic microchannels. *Chem. Eng. J.* **2012**, *188*, 86–97. [CrossRef]
27. Hashemi, S.E.; Lien, K.M.; Schnell, S.K.; Austbø, B. Thermodynamic analysis of different methanation reactors for biogas upgrading. *Comput. Aided Chem. Eng.* **2020**, *48*, 367–372. [CrossRef]
28. Sun, D.; Khan, F.M.; Simakov, D.S.A. Heat removal and catalyst deactivation in a Sabatier reactor for chemical fixation of CO_2: Simulation-based analysis. *Chem. Eng. J.* **2017**, *329*, 165–177. [CrossRef]
29. Sun, D.; Simakov, D.S.A. Thermal management of a Sabatier reactor for CO_2 conversion into CH_4: Simulation-based analysis. *J. CO_2 Util.* **2017**, *21*, 368–382. [CrossRef]
30. Kiewidt, L.; Thöming, J. Predicting optimal temperature profiles in single-stage fixed-bed reactors for CO_2-methanation. *Chem. Eng. Sci.* **2015**, *132*, 59–71. [CrossRef]
31. Faria, A.C.; Miguel, C.V.; Rodrigues, A.E.; Madeira, L.M. Modeling and Simulation of a Steam-Selective Membrane Reactor for Enhanced CO_2 Methanation. *Ind. Eng. Chem. Res.* **2020**, *59*, 16170–16184. [CrossRef]
32. Kampen, J.V.; Boon, J.; Berkel, F.V.; Vente, J.; Annaland, M.V.S. Steam separation enhanced reactions: Review and outlook. *Chem. Eng. J.* **2019**, *374*, 1286–1303. [CrossRef]
33. Diban, N.; Aguayo, A.T.; Bilbao, J.; Urtiaga, A.; Ortiz, I. Membrane Reactors for in Situ Water Removal: A Review of Applications. *Ind. Eng. Chem. Res.* **2013**, *52*, 10342–10354. [CrossRef]
34. Walspurger, S.; Elzinga, G.D.; Dijkstra, J.W.; Sarić, M.; Haije, W.G. Sorption enhanced methanation for substitute natural gas production: Experimental results and thermodynamic considerations. *Chem. Eng. J.* **2014**, *242*, 379–386. [CrossRef]
35. Faria, A.C.; Miguel, C.V.; Madeira, L.M. Thermodynamic analysis of the CO_2 methanation reaction with in-situ water removal for biogas upgrading. *J. CO_2 Util.* **2018**, *26*, 271–280. [CrossRef]
36. Najari, S.; Gróf, G.; Saeidi, S. Enhancement of hydrogenation of CO_2 to hydrocarbons via In-Situ water removal. *Int. J. Hydrogen Energy* **2019**, *44*, 24759–24781. [CrossRef]
37. Hillestad, M. Systematic staging in chemical reactor design. *Chem. Eng. Sci.* **2010**, *65*, 3301–3312. [CrossRef]
38. Fischer, K.L.; Langer, M.R.; Freund, H. Dynamic carbon dioxide methanation in a wall-cooled fixed bed reactor: Comparative evaluation of reactor models. *Ind. Eng. Chem. Res.* **2019**, *58*, 19406–19420. [CrossRef]
39. Lohmuller, R.; Schneider, H.; Watson, A. Methanation Process. U.S. Patent US4294932A, 13 October 1981.
40. Fogler, H.S. *Essentials of Chemical Reaction Engineering*; Prentice Hall: Upper Saddle River, NJ, USA, 2011.
41. Koschany, F.; Schlereth, D.; Hinrichsen, O. On the kinetics of the methanation of carbon dioxide on coprecipitated NiAl$(O)_x$. *Appl. Catal. B Environ.* **2016**, *181*, 504–516. [CrossRef]

42. Lunde, P.J.; Kester, F.L. Carbon dioxide methanation on a Ruthenium catalyst. *Ind. Eng. Chem. Process Des. Dev.* **1974**, *13*, 27–33. [CrossRef]
43. Aparicio, L.M. Transient Isotopic Studies and Microkinetic Modeling of Methane Reforming over Nickel Catalysts. *J. Catal.* **1997**, *165*, 262–274. [CrossRef]
44. Kee, R.J.; Coltin, M.E.; Glarborg, P.; Zhu, H. *Chemically Reacting Flow: Theory, Modeling, and Simulation*, 2nd ed.; John Wiley & Sons: Hoboken, NJ, USA, 2018; Chapter 3. [CrossRef]
45. Fuller, E.N.; Schettler, P.D.; Giddings, J.C. New method for prediction of binary gas-phase diffusion coefficients. *Ind. Eng. Chem.* **1966**, *58*, 18–27. [CrossRef]
46. Kotas, T.J. *The Exergy Method of Thermal Plant Analysis*; Exergon Publishing Company: London, UK, 2012.